

Flux Penetration in Superconducting Strip with Edge-Indentation

J. I. Vestgård, D. V. Shantsev, Y. M. Galperin and T. H. Johansen
*Department of Physics and Center for Advanced Materials and Nanotechnology,
 University of Oslo, P. O. Box 1048 Blindern, 0316 Oslo, Norway*

The flux penetration near a semicircular indentation at the edge of a thin superconducting strip placed in a transverse magnetic field is investigated. The flux front distortion due to the indentation is calculated numerically by solving the Maxwell equations with a highly nonlinear $E(j)$ law. We find that the excess penetration, Δ , can be significantly ($\sim 50\%$) larger than the indentation radius r_0 , in contrast to a bulk superconductor in the critical state where $\Delta = r_0$. It is also shown that the flux creep tends to smoothen the flux front, i.e. reduce Δ . The results are in very good agreement with magneto-optical studies of flux penetration into an $\text{YBa}_2\text{Cu}_3\text{O}_x$ film having an edge defect.

I. INTRODUCTION

Magnetic field penetrates type-II superconductors as a set of quantized flux lines – vortices. Macroscopically, the vortex matter can be considered as a “flux liquid”. An important feature of this matter is pinning of vortices leading to zero electrical resistance at zero temperature. The pinning results in a non-uniform distribution of magnetic flux forming a *critical state*. The critical state determines the macroscopic properties, e.g. the maximum current density and magnetic susceptibility, that are important for applications. According to the critical state model,¹ at any point of the sample the local value of the electrical current density is equal to its critical value, j_c , for a given magnetic field and temperature.

An interesting property of the critical state is that *local* material defects affect the field and current distributions on a *global* scale. For example, even a small non-superconducting cavity or an edge indentation create sample-spanning discontinuity lines where the current flow direction changes abruptly.² At a non-zero temperature, the critical state is relaxed due to flux creep that is conventionally described by a highly nonlinear current-voltage curve, $E \propto j^n$ where $n \gg 1$ and E is electric field. Nevertheless, the same tendency persists: a small cavity of size ℓ in a bulk superconductor perturbs the field distributions on a much larger scale of $\sim n\ell$.³ Many applications of superconductors are based on thin films where this tendency must be even stronger since the relation between the magnetic field and current is *nonlocal*.⁴ Usually this leads to poorer performance of superconducting devices whose global properties are deteriorated by numerous natural defects blocking the current flow. However, the same tendency can help control the flux motion on a global scale by patterning the superconductor with arrays of small holes designed, e.g., to guide the flux in a particular direction.^{5,6}

Surprisingly, a quantitative understanding on how a single local defect affects the flux penetration into a superconducting film is still rather poor. Even the simple case of an infinitely long thin strip with a semicircular edge-indentation is not solved. For a bulk super-

conductor in the critical state such an indentation creates an excess flux penetration exactly equal to the indentation radius.² However the nonlocal electrodynamics in thin films and hence the presence of Meissner currents in the flux-free regions make the picture much more complicated.⁷ It has been observed using magneto-optic imaging that the excess flux penetration in films can significantly exceed the size of the indentation it originates from.⁸ The physical mechanism behind this enhancement is however not yet understood. It could be related to the effect of thin-film geometry, to the flux creep or to thermal instabilities nucleated at the indentation.

This work aims to clarify this question by presenting a detailed study of flux penetration into a strip with a semicircular edge-indentation in the flux creep regime. We determine how the excess penetration depends on the size of the indentation, the applied magnetic field and the creep exponent n .

II. MODEL

Consider a thin superconducting strip of thickness d placed in a transverse magnetic field. The strip is infinite in the y -direction, has the width $2w \gg d$ in the x -direction and a semicircular indentation with radius r_0 at the edge, see Fig. 1. The flux dynamics in the creep regime is conventionally described using a local relation between electric field \mathbf{E} and current density \mathbf{j} ,^{9,10,11}

$$\mathbf{E} = \rho \mathbf{j}, \quad (1)$$

with a highly nonlinear resistivity

$$\rho = \rho_0 (j/j_c)^{n-1}, \quad (2)$$

which does not explicitly depend on the magnetic induction B . Here ρ_0 is a constant, j_c is the critical current density, while n is the creep exponent, $n \gg 1$. This exponent can be related to the activation energy U for thermal depinning as $n \sim U/kT$. Hence, large n means small creep, and the Bean critical state model¹ is regained in the limit $n \rightarrow \infty$.

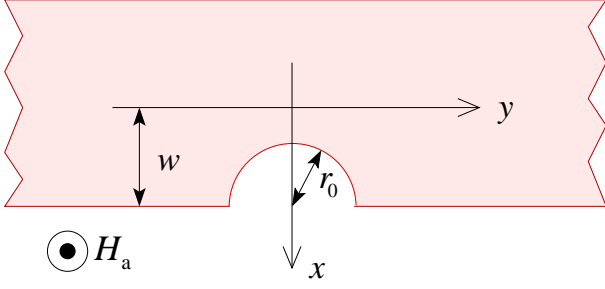


FIG. 1: A superconducting strip of width $2w$ with a semicircular indentation of radius r_0 in transverse field H_a .

For numerical simulations of flux penetration into the strip we use the formalism developed by Brandt^{4,9,11,12,13,14,15,16,17} that can be applied to thin type-II superconductors of various shapes. For a thin superconductor, it is appropriate to look at length scales larger than the thickness d , and introduce a sheet current

$$\mathbf{J}(\mathbf{r}) = \int_{-d/2}^{d/2} dz \mathbf{j}(\mathbf{r}, z),$$

where $\mathbf{r} = (x, y)$ are in-plane coordinates. Due to the current conservation, $\nabla \cdot \mathbf{J} = 0$, the sheet current can be expressed through a scalar function $g(\mathbf{r})$ as

$$\mathbf{J} = \nabla \times \hat{z} g \quad (3)$$

where g has the interpretation of the local magnetization.⁹ Substituting the current from Eq. (3) into the Biot-Savart law one arrives at a non-local relation between B_z and g ,

$$B_z(\mathbf{r}, z) = \mu_0 H_a + \int_A d^2 r' Q(\mathbf{r}, \mathbf{r}', z) g(\mathbf{r}'). \quad (4)$$

Here H_a is the applied field and A is the sample area. The integral kernel is equal to the field of a dipole of unit strength,

$$Q(\mathbf{r}, \mathbf{r}', z) = \frac{\mu_0}{4\pi} \frac{2z^2 - (\mathbf{r} - \mathbf{r}')^2}{[z^2 + (\mathbf{r} - \mathbf{r}')^2]^{5/2}}. \quad (5)$$

The integral Eq. (4) with kernel Eq. (5) is divergent at $\mathbf{r} \rightarrow \mathbf{r}'$ and $z \rightarrow 0$. In a numerical procedure, the divergence can be handled in three ways: (i) by keeping a finite z during the calculation;¹⁸ (ii) by working in the Fourier space;¹¹ (iii) by converting the integral to a matrix form and using the flux conservation to determine the diagonal elements.^{12,16,17} Here we use the third method. Since, for $H_a = 0$, the total flux through the $z = 0$ plane is zero, the kernel should have the property $\int d^2 r Q(\mathbf{r}, \mathbf{r}', 0) = 0$. This yields

$$\frac{1}{\mu_0} B_z(\mathbf{r}) = H_a + g(\mathbf{r}) C(\mathbf{r}) - \int_A \frac{d^2 r'}{4\pi} \frac{g(\mathbf{r}') - g(\mathbf{r})}{|\mathbf{r} - \mathbf{r}'|^3}, \quad (6)$$

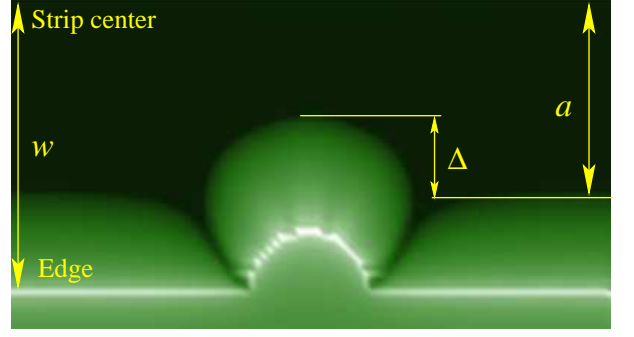


FIG. 2: The simulated flux density map in a strip of width $2w$, with a semicircular indentation of radius $r_0 = 0.2w$, in applied field $H_a = 0.3J_c$, $n = 19$, and ramped with a rate $\mu_0 \dot{H}_a = \rho_0 J_c / wd$. Note that Δ is not equal to r_0 .

where the scalar function C is an integral over the area *outside* the superconductor

$$C(\mathbf{r}) = \int_{\text{outside}} \frac{dr'^2}{4\pi |\mathbf{r} - \mathbf{r}'|^3}. \quad (7)$$

For a uniform strip of width $2w$ it yields

$$C_{\text{strip}}(x) = \frac{1}{\pi} \frac{w}{w^2 - x^2}. \quad (8)$$

In addition, the indentation gives a contribution from the semicircle, which is calculated numerically from Eq. (7).

In the following we use an equidistant square grid and ascribe the same area s to each grid point. The discrete version of the kernel then acquires the form¹⁷

$$\frac{Q_{ij}}{\mu_0} = \delta_{ij} \left(\frac{C_i}{s} + \sum_l q_{il} \right) - q_{ij}, \quad (9)$$

where $q_{ij} = 1/4\pi |\mathbf{r}_i - \mathbf{r}_j|^3$ for $i \neq j$ and $q_{ii} = 0$. All elements of the discrete kernel Eq. (9) are nondivergent and the flux conservation, $\int d^2 r B(\mathbf{r}) = 0$, is guaranteed. Relating the magnetic field and the current by the Faraday's law, and using the inverted Biot-Savart law one obtains the dynamic equation for the local magnetization:

$$\dot{g}(\mathbf{r}, t) = \int_A d^2 r' Q^{-1}(\mathbf{r}, \mathbf{r}') [\hat{f}g(\mathbf{r}', t) - \dot{H}_a(t)], \quad (10)$$

where

$$\hat{f}g \equiv \nabla \cdot (\rho \nabla g) / d\mu_0.$$

For discrete formulation of the problem the inverse kernel Q^{-1} is just the inverse of the matrix Eq. (9), hence the matrix must be calculated and inverted only once.

III. RESULTS AND DISCUSSION

a. Magnetic field and current The simulations were performed by ramping the applied field at a constant

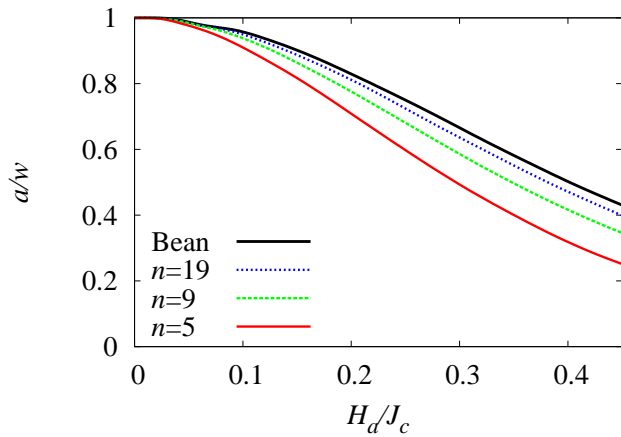


FIG. 3: Evolution of flux penetration depth a as the applied field is ramped with a constant rate $\mu_0 \dot{H}_a = \rho_0 J_c / wd$. Stronger flux creep, i.e. smaller n , leads to deeper penetration. The Bean limit is $n = 101$.

rate $\mu_0 \dot{H}_a = \rho_0 J_c / wd$, starting at zero field and a flux-free strip. The flux penetrates from the edges forming well-defined flux fronts that move towards the strip center as the applied field increases. Shown in Fig. 2 is a typical result of the flux density distribution presented as seen in a magneto-optical image, i.e., the image brightness represents the magnitude of the perpendicular magnetic field. The sample edge is seen as a bright line, i.e., the flux density is highest at the edge.

Far from the indentation the flux penetration front is straight, and leaves a fraction a/w of the strip in the flux-free Meissner state, seen here as a black region. The penetration of this straight front versus applied field is shown in Fig. 3 for different values of the creep exponent. For large n the simulations approach the Bean-model result,⁴ $a_{\text{Bean}} = w / \cosh(\pi H_a / J_c)$, while for smaller n , i.e., stronger flux creep, the penetration is deeper, all as expected for a strip with straight edges.

Near the indentation the flux penetration largely follows the circular shape. At both sides of the indentation there are dark regions of reduced flux density. As penetration gets deeper these will become narrow d -lines, where the current stream lines make sharp turns.² In the Bean limit $n \rightarrow \infty$, the d -lines of semicircular indentations have parabolic shape. With finite n the parabolic shape is only approximated. However, the main effect of the indentation is that it pushes magnetic field deeper into the sample. In order to quantify this we define the excess penetration Δ as the difference between the deepest penetration and the penetration far away from the indentation. Fig. 4 shows how Δ evolves with increasing H_a . Evidently, the excess penetration is not equal to the indentation radius, r_0 , as in the case of the bulk Bean model.^{2,3,19} Moreover, Δ turns out to be field-dependent. Initially, Δ increases, then reaches a maximum followed by a decrease at larger H_a . This surpris-

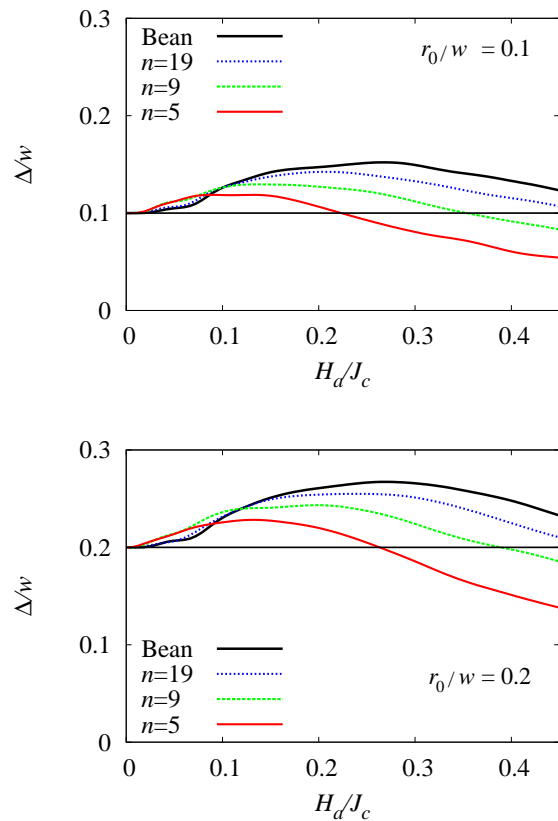


FIG. 4: Evolution of the indentation-induced excess penetration, Δ , as a function of applied field. The two panels correspond to different indentation radii, $r_0/w = 0.1$ and 0.2 , respectively; $\mu_0 \dot{H}_a = \rho_0 J_c / wd$.

ing non-monotonous behaviour is supported by magneto-optical measurements of the flux penetration in a uniform $\text{YBa}_2\text{Cu}_3\text{O}_x$ film containing an edge defect, see Fig. 5. The film was shaped as a strip of half-width $w = 0.4$ mm, and the figure shows the flux distribution at 25 K for 3 different applied fields. In (a) the field was very small, $\mu_0 H_a = 3$ mT, creating negligible penetration so that the actual shape of the defect appears in the image as the bright "bay area" inside the strip. In this state the excess penetration is equal to the depth of the defect, and measures $\Delta = 80 \mu\text{m}$. In (b) and (c) the applied field is 17 mT and 36 mT, respectively, and the corresponding excess penetration is $\Delta = 115 \mu\text{m}$ and $100 \mu\text{m}$. This gives for $\Delta/w = 0.20, 0.29$ and 0.25 , demonstrating an excess penetration that exceeds the depth of the indentation by nearly 40 %, in very good agreement with the Bean model results plotted in Fig. 4.

The Fig. 4 includes the behaviour of Δ/w for two different r_0/w . Comparing the two panels we see that larger indentations produce a larger Δ . However, the relative excess penetration, Δ/r_0 is larger for the *smaller* indentation. The excess penetration can exceed the indentation depth by almost 50 % for $r_0 = 0.1w$ and large values of

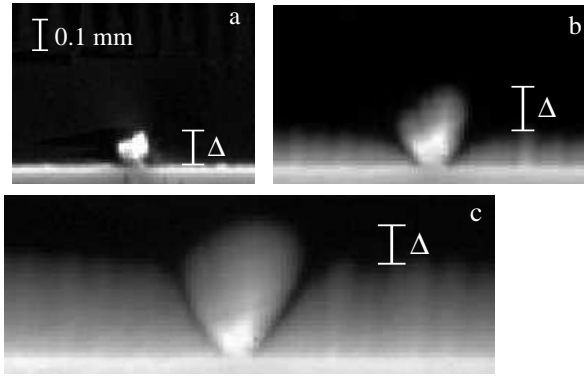


FIG. 5: Magneto-optical images of flux penetration into an $\text{YBa}_2\text{Cu}_3\text{O}_x$ strip with a defect at the edge. Only the lower half of the strip is shown. In (a), (b) and (c) the applied fields was 3, 17 and 36 mT, respectively. The excess flux penetration, Δ , is maximal at the intermediate field, in agreement with simulations.

n . For smaller values of the creep exponent one always finds smaller Δ , implying that creep tends to smoothen perturbations in the flux front.³

Our results demonstrate that an indentation in a thin film affects the flux distribution in a stronger and more complex way than it does in bulk superconductors. This must be due to the non-local electrodynamics of thin films, and in particular due to the presence of Meissner currents in the flux free regions. These Meissner currents do not make the same sharp turns as the critical currents in the flux penetrated region, see Fig. 6 and also Refs. 9,11. As a result, the Meissner currents concentrate in front of the indentation where their density reaches j_c and hence leads to even deeper flux penetration. This is why the flux front near the indentation advances faster than in the rest of the film. This accelerated advancement eventually terminates when the penetration depth becomes comparable to the strip halfwidth. The reason is simply that in the limit of full penetration all flux fronts reach the middle of the strip and hence $\Delta \rightarrow 0$.

b. Electric field The Lorentz force pushing magnetic flux is directed perpendicular to the local current density. Even a small indentation distorts the current stream lines over a large area, and hence significantly modifies the trajectories of flux motion. In particular, all the flux arriving to the fan-shaped region rooted at the indentation must have entered the sample through this indentation, see Fig. 5. It creates a dramatic local enhancement of electric field since E is a direct measure of the intensity of flux traffic.

Analytical solution for the electric field distribution around an indentation in thin films is not available. Therefore the results obtained for the case of a slab are often utilized as approximations also for films.^{3,14,20} We will now analyze to what extent such estimates are valid by comparing them with our simulation results for a strip.

In the fan-shaped region that originates from the semi-circular indentation, the electric field can be found by

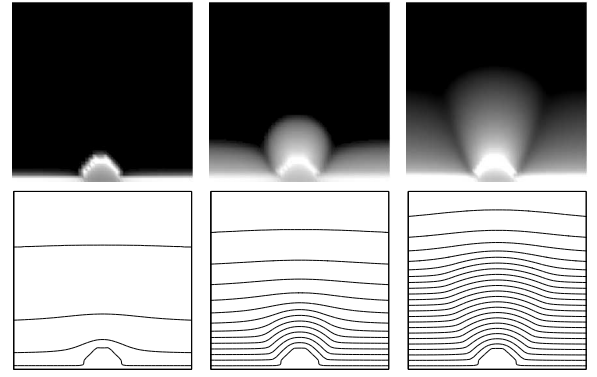


FIG. 6: Simulated flux distributions (top) and current stream lines (bottom) in an increasing applied field, where $r_0 = 0.1w$ and the other parameters the same as in Fig. 2. From left, the values of H_a are $0.05J_c$, $0.2J_c$, and $0.4J_c$ with corresponding values of a $0.98w$, $0.8w$, and $0.5w$.

solving the Maxwell equation $\nabla \times \mathbf{E} = -\dot{\mathbf{B}}$ in cylindrical coordinates. Since the evolution of B -distribution is usually not very far from the Bean model, one can assume $\dot{\mathbf{B}} = \mu_0 \dot{H}_a$, which leads to the solution¹⁴

$$E_1(x) = \frac{\mu_0 \dot{H}_a}{2} \left[\frac{(w - a + r_0)^2}{w - |x|} - (w - |x|) \right] \quad (11)$$

for $|x| > a - r_0$ and zero for $|x| < a - r_0$. Far away from the indentation the solution of the same equation in cartesian coordinates, $\partial_x E = -\mu_0 \dot{H}_a$, is

$$E_0(x) = \mu_0 \dot{H}_a (|x| - a) \quad (12)$$

for $|x| > a$ and zero for $|x| < a$. Note that the width w enters Eq. (11) only because of the specific choice of the x -coordinate, where the edge is located at $x = w$. Replacement $x \rightarrow x + w$ removes the w -dependence.

Figure 7 compares $E_0(x)$ and $E_1(x)$ with the simulated electric field profiles. The quantitative agreement is poor, though the shape of profiles (both across the indentation and away from it) is fairly well reproduced, in agreement with Ref. 8. The expected enhancement of E due to indentation is also obvious. The formulas above predict the relative enhancement for the peak values $E_1^{(\max)}/E_0^{(\max)} = (w - a)/2r_0 + 1$ for a bulk sample. One can see from the plot that the effect of indentation is even stronger for thin films: the ratio $E_1^{(\max)}/E_0^{(\max)}$ is slightly higher and the excess penetration is larger (the flux front here corresponds to the point where $E(x) = 0$).

A locally enhanced electric field near edge indentations and hence enhanced Joule heating is predicted to facilitate nucleation of a thermal instability.^{14,20} The instability in thin superconductors is usually observed in form of macroscopic dendritic flux avalanches²¹ or macroscopic uniform flux jumps²². However, a third scenario is also possible when a series of *microscopic* flux avalanches repeatedly take place in the same region, each leading to a small advancement of the flux front.²³ It creates an

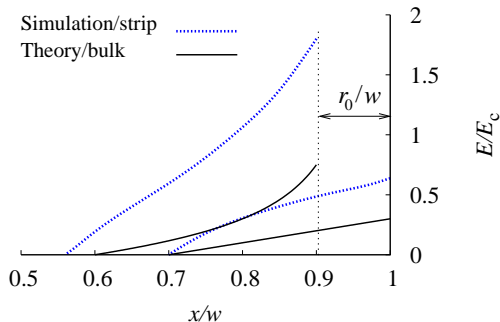


FIG. 7: Electric field profiles across the indentation and far away from it. Solid lines: Eqs. 11 and 12 for a bulk superconductor. Dashed lines: simulations for a thin-film strip; the parameters are the same as for Fig. 2 except that $r_0 = 0.1w$ and $H_a/J_c = 0.25$. $E_c = \rho_0 J_c/d$. A strong field enhancement near the indentation is clearly seen.

additional front distortion since the avalanches are expected to be larger and occur more frequently at the indentation, where the local E is maximal. Experimentally the individual avalanches can be very small, and hence it is not easy to determine whether the thermal effects contribute to an observed front distortion. To identify the penetration mechanism one can compare the observed flux profiles with the simulations. The maximal excess penetration due to non-thermal effects is found to be 150 % of the indentation radius for our parameters. Consequently, when the observed excess penetration is larger, the flux penetration probably occurs via thermal micro-avalanches.

IV. CONCLUSIONS

We have numerically solved the Maxwell equations to describe flux penetration into a thin superconducting strip with an edge-indentation and analyzed the time evolution of flux front in an increasing applied field, H_a . The excess penetration, Δ , due to the indentation is not equal to the indentation radius, r_0 , in contrast to the well-known case of a bulk superconductor in the Bean model. Three different mechanisms that influence

the excess penetration were analyzed. (i) The nonlocal electrodynamics in films leads to a characteristic $\Delta(H_a)$ dependence with a smooth peak. The ratio Δ/r_0 at the peak equals 1.5 when r_0 is 0.1 of the strip half-width and becomes even larger for smaller r_0 . (ii) The flux creep always tends to smoothen the flux front and decrease the excess penetration. (iii) Thermal flux avalanches are more likely to occur at the indentation, which can increase the apparent front distortion. Our results can be very helpful in order to identify which of these three mechanisms is the dominant one in a concrete experiment.

Acknowledgments

We thank C. Romero and Ch. Jooss for fruitful discussions. This work was supported financially by The Norwegian Research Council, Grant No. 158518/431 (NANOMAT) and by FUNMAT@UIO.

APPENDIX A: NUMERICAL DETAILS

The simulations are carried out on an equidistant square grid with $N \times N$ points, $x_m = w(2m + 1)/N - w$ and $y_n = w(2n + 1)/N - w$, for $0 \leq m, n < N$. The system has two symmetries that must be incorporated in the kernel: first, the periodic boundary, which means that we must add a mirror strips at $x < -w$ and $x > w$. Second, the symmetry around $x = 0$. The latter means that we can work with half the kernel.¹¹ The simulations use a grid size of $N = 100$, which means that a 5000×5000 matrix must be put in memory and inverted. The memory consumption is the main limiting factor of the simulations. The kernel is stable, so there is no need for additional smoothening. For most exponents a pure power law is used, but for the Bean limit, $n = 101$, a cutoff on the resistivity $\rho < \rho_{\max}$ was necessary to ensure stability. The flux front position was determined at every time step and then smoothened as a function of time. It allows the front position to be determined with an accuracy much better than the distance between two grid points.

-
- ¹ C. P. Bean, Rev. Mod. Phys. **36**, 31 (1964).
 - ² A. M. Campbell and J. Evetts, *Critical Currents in Superconductors* (Taylor and Francis LTD, London, 1972).
 - ³ A. Gurevich and M. Friesen, Phys. Rev. B **62**, 4004 (2000).
 - ⁴ E. H. Brandt and M. Indenbom, Phys. Rev. B **48**, 12893 (1993).
 - ⁵ R. Wördenweber, P. Dymashevski, and V. R. Misko, Phys. Rev. B **69**, 184504 (2004).
 - ⁶ V. V. Yurchenko, R. Wördenweber, Y. M. Galperin, D. V. Shantsev, J. I. Vestgård, and T. H. Johansen, Physica

- C **437-438**, 357 (2006).
- ⁷ J. Eisenmenger, P. Leiderer, M. Wallenhorst, and H. Dötsch, Phys. Rev. B **64**, 104503 (2001).
- ⁸ T. Schuster, H. Kuhn, and E. H. Brandt, Phys. Rev. B **54**, 3514 (1996).
- ⁹ E. H. Brandt, Phys. Rev. Lett. **74**, 3025 (1995).
- ¹⁰ E. Zeldov, N. M. Amer, G. Koren, A. Gupta, and M. W. McElfresh, Appl. Phys. Lett. **56**, 680 (1990).
- ¹¹ E. H. Brandt, Phys. Rev. B **52**, 15442 (1995).
- ¹² E. H. Brandt, Phys. Rev. B **46**, 8628 (1992).

- ¹³ T. Schuster, H. Kuhn, E. H. Brandt, M. V. Indenbom, M. Kläser, G. Müller-Vogt, H.-U. Habermeier, H. Kronmüller, and A. Forkl, *Phys. Rev. B* **52**, 10375 (1995).
- ¹⁴ R. G. Mints and E. H. Brandt, *Phys. Rev. B* **54**, 12421 (1996).
- ¹⁵ E. H. Brandt, *Phys. Rev. B* **55**, 14513 (1997).
- ¹⁶ E. H. Brandt, *Phys. Rev. B* **64**, 024505 (2001).
- ¹⁷ E. H. Brandt, *Phys. Rev. B* **72**, 024529 (2005).
- ¹⁸ K. A. Lörincz, M. S. Welling, J. H. Rector, and R. J. Wijngaarden, *Physica C* **411**, 1 (2004).
- ¹⁹ T. Schuster, M. V. Indenbom, M. R. Koblishka, H. Kuhn, and H. Kronmüller, *Phys. Rev. B* **49**, 3443 (1994).
- ²⁰ A. Gurevich, *Appl. Phys. Lett.* **78**, 1891 (2001).
- ²¹ D. V. Denisov, D. V. Shantsev, Y. M. Galperin, E.-M. Choi, H.-S. Lee, S.-I. Lee, A. V. Bobyl, P. E. Goa, A. A. F. Olsen, and T. H. Johansen, *Phys. Rev. Lett.* **97**, 077002 (2006).
- ²² R. Prozorov, D. V. Shantsev, and R. G. Mints, *Phys. Rev. B* **74**, 220511(R) (2006).
- ²³ D. V. Shantsev, A. V. Bobyl, Y. M. Galperin, T. H. Johansen, and S. I. Lee, *Phys. Rev. B* **72**, 024541 (2005).